

Adsorption-Induced Expansion of Graphene Oxide Frameworks with Covalently Bonded Benzene-1,4-diboronic Acid: Numerical Studies

Todd N. Lombardi,* Joseph C. Schaeperkoetter, Alberto Albesa, and Carlos Wexler*



Cite This: *ACS Omega* 2022, 7, 11980–11987



Read Online

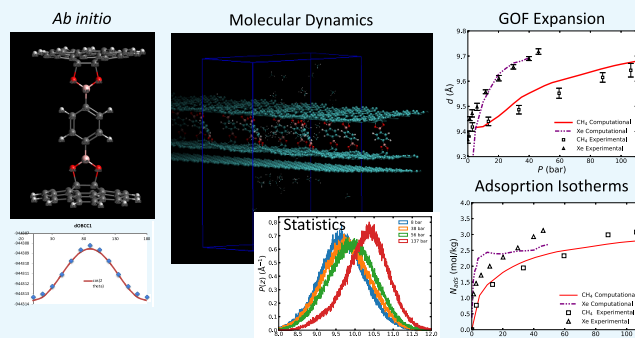
ACCESS |

Metrics & More

Article Recommendations

Supporting Information

ABSTRACT: Graphene oxide frameworks (GOFs) are interesting adsorbent materials with well-defined slit-shaped pores of almost monodisperse separation of ~ 1 nm between graphene-like layers; however, the exact nature of the structure has remained undetermined. Recently, GOFs were observed to swell monotonically upon the adsorption of methane and xenon under supercritical conditions. Here, we present the results of molecular dynamics simulations of the adsorption of methane and xenon for various proposed GOF structures based upon force fields based on *ab initio* B3LYP density functional theory calculations. The simulations reproduce well both the adsorption isotherms and the expansion of the interlayer spacing for methane and xenon for a model of GOFs formed by covalently bonded benzene-1,4-diboronic acid oriented at quasirandom angles with respect to the graphene layers.



1. INTRODUCTION

Carbon-based porous materials have been studied extensively for their potential for energy storage in the form of hydrogen or methane, other gas storage applications, and gas separation (e.g., sequestration of carbon dioxide). The reason for this interest in carbon nanostructures is their tremendous variety, which includes various amorphous activated carbons,^{1–3} metal organic frameworks (MOFs),^{4,5} covalent organic frameworks (COFs), and more recently graphene oxide frameworks (GOFs). In general, the storage capacity of these materials is roughly proportional to their specific surface area (SSA, which often is close to $\sim 2600 \text{ m}^2/\text{g}$ of graphene) and is maximal for pore sizes in the neighborhood of ~ 1 nm. For maximal storage delivery, Bhatia and Myers⁶ demonstrated that there is an optimal adsorption enthalpy of $\sim 18 \text{ kJ/mol}$ for room-temperature operation, and Kuchta et al. demonstrated that an optimum adsorbent should be homogeneous.⁷

Graphene oxide frameworks (GOFs) are a particularly promising structure for various physicochemical processes. GOFs are formed when graphene oxides are linked by different functional groups,⁸ thus producing a layered structure^{9–11} with possibly tunable pore widths depending upon the type of binder used, which may be optimized, e.g., for storage of a particular gas.^{9,12–15} Notably, similar layered materials have been produced by silylation reactions.^{16,17} A detailed understanding of the structure of GOFs at the atomic level is thus desired to produce future high-performance nanoporous materials for applications such as gas storage, separation, catalysis, supercapacitors, batteries, etc.

In this paper, we focus on the structural properties of a type of GOF formed using an intercalation procedure originally proposed by Burress et al.⁹ and reproduced by Mercier et al.¹¹ and Schaeperkoetter et al.:¹⁸ the dissolution of benzene-1,4-diboronic acid (DBA) in methanol and then intercalating the DBA into graphite oxide (GO), which lead to GOFs with SSA of ≈ 400 to $1000 \text{ m}^2/\text{g}$ and interlayer distances of $\sim 9 \text{ \AA}$.

Originally, there were three competing models of GOFs (possibly) linked by DBA molecules. Burress et al.⁹ assumed that GOFs were composed of graphene oxide layers separated by rigid DBA linkers with oxygen atoms covalently bonded to both graphene planes and benzene diboronic linkers; we refer to this structure as (i) “covalent pillared GOF” (CP-GOF). Mercier et al.,¹¹ however, posited that the proposed structures would be unlikely given the characteristic size of the DBA linkers (i.e., the pores would be larger than observed experimentally), and that their observations of swelling of the pores by as much as 50% in methanol seemed unlikely given the strength of typical covalent bonds.¹¹ Thus, Mercier et al.¹¹ proposed two alternative models for the GOF-DBA structure: (ii) the “van der Waals GOF” (vdW-GOF), where covalent bonds are formed alternatively on alternating walls of

Received: January 8, 2022

Accepted: March 4, 2022

Published: March 30, 2022



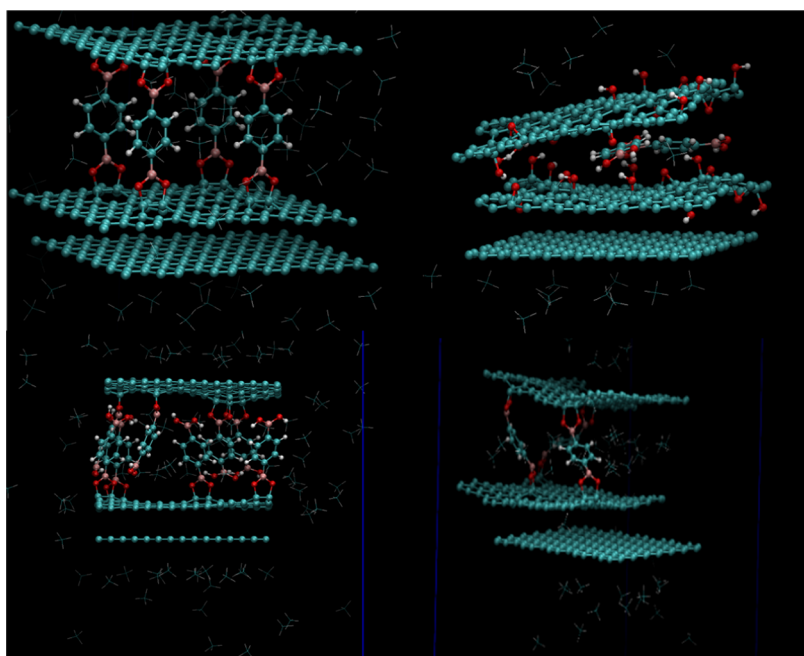


Figure 1. Postulated models of GOFs: the covalent pillared GOF (top left), the fluid DBA (top right), the vdW-GOF (bottom left), and the covalent angled GOF (bottom right). A stabilizing layer is included at the bottom to simulate an underlying solid structure (see also refs^{9–11, 18}

the pore, and van der Waals interactions between the DBA tails securing the structure together and a (iii) “fluid-DBA” model (fDBA-GOF), where DBA molecules possibly interacting via enhanced electrostatic interactions with polar groups in the GO sustain the two GO planes apart. As we shall see, our analysis rules out models (i)–(iii) and proposes an alternative model: (iv) “covalent angled GOF” (CA-GOF), which is compatible with experimental data. The models are depicted in Figure 1.

A significant breakthrough came in 2019 when Schaeperkoetter et al.¹⁸ probed these structures by *in situ* neutron diffraction during supercritical adsorption of various gases at pressures in the 0–140 bar range. Thermal neutrons from the 10 MW University of Missouri Research Reactor were particularly well suited for structural investigations of GOFs¹⁹ since they can readily penetrate the thick high-pressure aluminum sample cell (in contrast, X-ray scattering cross section increases with Z^2 , making it very difficult to probe carbon structures surrounded by thick metal walls).

Schaeperkoetter observed that the interlayer spacing d_{001} increases gradually and monotonically as a function of pressure for methane, hydrogen, and xenon during supercritical adsorption.¹⁸ The gradual change did not fit the typical either “gate-opening” transitions or other contraction/swelling of nanoporous materials that had been previously observed under *subcritical* adsorption^{20–26}—in fact, in gate-opening systems, a bulk phase change usually precedes the gate-opening such as capillary condensation, but our gas’s isotherms were measured at supercritical conditions making a bulk phase change impossible. Another notable observation was that this swelling could be mapped onto a common expansion curve for all three gases using a scaling directly related to the van der Waals gas–solid interaction energy¹⁸ in a manner similar to the law of corresponding states for gases.^{27,28}

As we shall see below, our simulations of the adsorption of methane and xenon in the four GOF-DBA models proposed

are consistent only with the CA-GOF model shown in Figure 1 (bottom right panel).

2. METHODOLOGY

In this work, we analyze by means of molecular dynamics (MD) simulations the behavior of various models (Figure 1) of GOF-DBA under conditions similar to those of the experiments of Schaeperkoetter et al.:¹⁸ methane and xenon pressures in the 0–120 bar range at room temperature ($T = 300$ K). All simulations were completed using the NAMD2²⁹ MD code and analyzed using visual molecular dynamics (VMD) and various TCL scripts.³⁰ Interactions were cutoff for distances larger than 12 Å, and a neighbors’ list with a radius of 14 Å was maintained for accelerated calculations of forces. For each run, 5000 steps of energy minimization were performed, followed by $3,000,000 \times 1$ fs steps (i.e., 3 ns) of MD simulations in the canonical (N, V, T) ensemble using a velocity rescaling thermostat applied to all atoms (except for a single fixed stabilizing layer) every 20 fs with configurations saved for analysis every 1000 time steps (i.e., every 1 ps). The last 2 ns of each simulation was used for calculations of time averages (all simulations equilibrated in less than 0.5 ns). All simulations were performed inside a $21.3 \text{ \AA} \times 37.2 \text{ \AA} \times 50 \text{ \AA}$ parallelepiped box with periodic boundary conditions (PBC) in all directions; see Figure 2.

In each simulation, the GOF structure (models i, ii, iv), GO, and DBA (model iii) were simulated fully atomistically, and the atoms were allowed to move with the exception of a fixed graphene bottom layer that simulates a solid graphite substrate, increases the stability of the simulation, and facilitates the analysis by keeping the structures roughly aligned parallel to the xy plane. This is a reasonable model since GOF samples have SSAs of ≈ 400 to $500 \text{ m}^2/\text{g}$ ¹⁸ compared to graphene’s theoretical surface area of $2600 \text{ m}^2/\text{g}$.

The gases (methane, xenon) were also simulated fully atomistically. The number of gas molecules $N_{\text{met}} \in [0, 400]$,

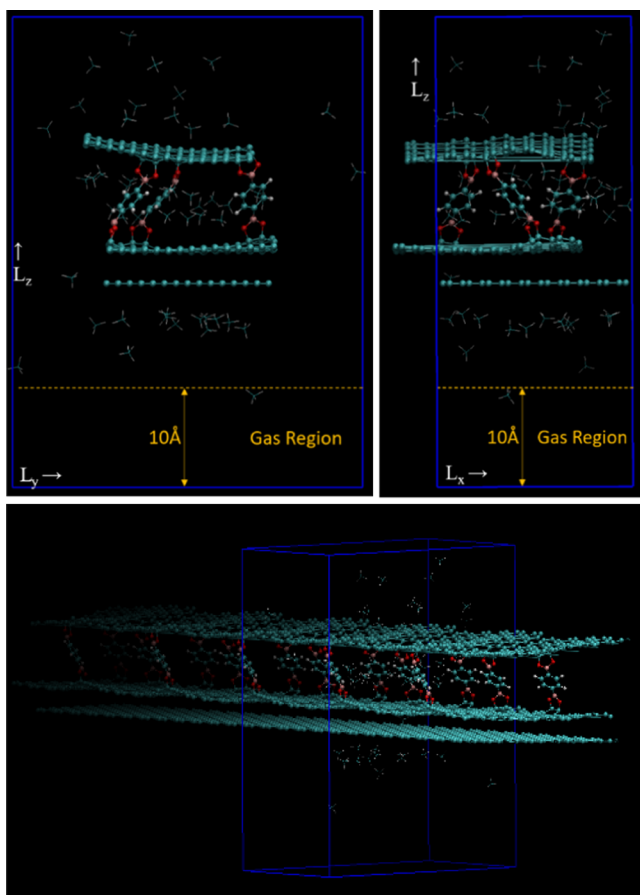


Figure 2. Head on view of a typical system along the x -axis (top left) showing regions (small regions (small and large y)) where gas molecules can transfer between the pore and gas phases. The system viewed along the y -axis (top right) shows carbon atoms in GOF bonded across the PBC. The “Gas Regions” in yellow, situated farther than the potential cutoff distance (12 Å) from the GOF, depict where the gas density is measured³² and the pressure calculated using NIST’s Thermophysical Properties of Fluid Systems database.³¹ The bottom panel illustrates the “strip” shape of the simulated GOF, i.e., infinite in the x - but finite in the y -direction.³²

$N_{\text{Xe}} \in [0, 400]$ was varied, and the pressure calculated using NIST’s Thermophysical Properties of Fluid Systems database³¹ from gas densities averaged far from the GOF (and DBA), i.e., in the bottom 10 Å of the simulation box; see Figure 2 and ref 32.³²

For interactions, we used the CHARMM22 force field³³

$$V = V_{\text{bond}} + V_{\text{angle}} + V_{\text{dihed}} + V_{\text{nb}} \quad (1)$$

The bond term is modeled in the harmonic form

$$V_{\text{bond}} = \sum_{\text{bonds}} k_b(b - b_0)^2 \quad (2)$$

where b is the bond length between a pair (1–2) of atoms, b_0 is the equilibrium bond length, and k_b is the bond force constant. To avoid unnecessary short time scales, C–H bonds were made rigid ($b = b_0$) using the RATTLE algorithm,³⁴ which allowed a time step of 1 fs. The second term accounts for the angle deformation

$$V_{\text{angle}} = \sum_{\text{angles}} (k_\theta(\theta - \theta_0)^2 + k_{\text{UB}}(S - S_0)^2) \quad (3)$$

where θ is the angle between a sequence of three bonded atoms, θ_0 is the bond-angle equilibrium value, k_θ is the angular harmonic stiffness constant, S_0 is the equilibrium distance between 1 and 3 pairs, and k_{UB} is the Urey–Bradley constant. The third term accounts for four-body dihedral torsion contributions

$$V_{\text{dihed}} = \sum_{\text{dihedrals}} k_\chi(1 + \cos(n\chi - \delta)) \quad (4)$$

where χ is the dihedral angle formed by a sequence of four bonded atoms, k_χ is the torsional stiffness, n is the multiplicity factor, and δ is the phase shift. The final term makes up the nonbonded interactions derived from two-body interactions for atom pairs either in the same or a different molecule and adatom–substrate pair interactions

$$V_{\text{nb}} = \sum_{i,j} \frac{q_i q_j}{4\pi\epsilon_0 r_{ij}} + \sum_{i,j} \epsilon_{ij} \left[\left(\frac{r_{\min,ij}}{r_{ij}} \right)^{12} - 2 \left(\frac{r_{\min,ij}}{r_{ij}} \right)^6 \right] \quad (5)$$

which are applied only to atom pairs separated by at least three bonds,³⁵ with 1–4 interactions modified by a scaling factor of 0.4.^{35,36} Here, q_i are the Mulliken partial atomic charges, r_{ij} are the interatom distances, ϵ_0 is the dielectric constant, ϵ_{ij} is the Lennard-Jones potential depth, and $r_{\min,ij}$ is the distance of the Lennard-Jones minimum. For heterogeneous atom pairs, we use the Lorentz–Berthelot combination rules³⁷

$$\epsilon_{ij} = \sqrt{\epsilon_i \epsilon_j}, \quad r_{\min,ij} = \frac{r_{\min,i}}{2} + \frac{r_{\min,j}}{2} \quad (6)$$

All LJ potentials were taken out to a pair separation of $r_l = 10$ Å and then smoothly diminished to zero at a cutoff distance $r_c = 12$ Å. Coulomb interactions were calculated using the particle mesh Ewald (PME) summation method.³⁸

In this work, the values of potential parameters are the result of a comprehensive study combining *ab initio* density functional theory (DFT/B3LYP)^{39–42} calculations using the Gaussian09 code⁴³ (including a base study, geometry optimization, variation of geometric parameters to determine elastic constants) and the CGenFF database^{44,45} for the dispersion terms. The methodology of the *ab initio* study and values of the interaction parameters used in this work are listed in the Supporting Information (see Tables S1 and S2; Figures S1 and S2).

3. RESULTS

3.1. Model Descriptions. MD simulations of the adsorption of methane and xenon were performed for the models of GOFs described above (see Section 1 and Figure 1):

For model (i) CP-GOF⁹, a number of DBA molecules (3 or 4 in our simulation box, as per the experimental B/C ratios of GOF samples^{9–11,18}) are covalently linked to both sides of the pore through C–O bonds (eq 2) to graphene at sites that are almost exactly on top of each other (Figure 1, top left). This results in a layer separation $d_{001} = 10.6$ Å in disagreement with the experimental neutron diffraction results for d_{001} : between 9.30 Å (*in vacuo*) and 9.75 Å ($P_{\text{Xe}} = 40$ bar)¹⁸ (note that in ref 18 $d_{001} = 10.3$ Å using X-ray diffraction, but this result is for samples in “wet” air, consistent with observations in ref 11). The covalent pillared GOF structures were unsurprisingly very stable and rigid and, as we shall see, showed no expansion during gas adsorption due to the substantial rigidity of the C–O covalent bonds and within the DBA itself against stretching.

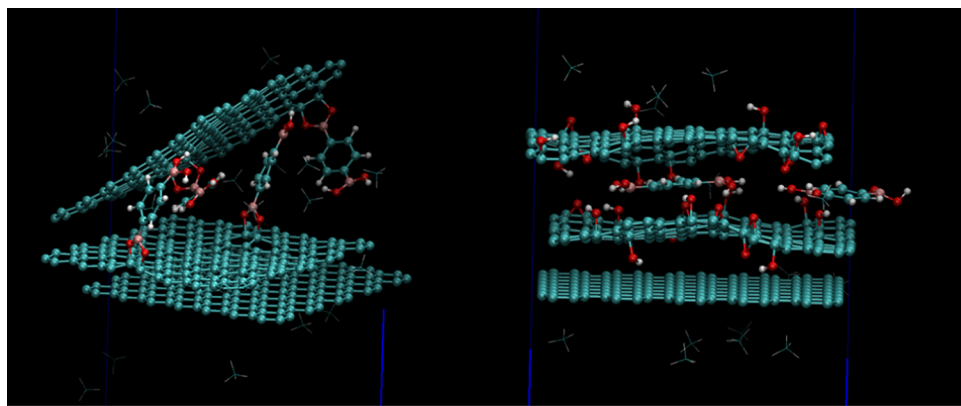


Figure 3. Typical collapsed van der Waals GOF (left) and fluid-DBA (right) models. These configurations almost completely excluded any gas molecules from adsorbing inside the pores.

For model (ii) vdW-GOF11, we also placed 2–4 DBA molecules (again consistent with experimental B/C ratios^{9–11,18}) but bonded them through C–O bonds to alternate sides, allowing nonbonded (eq 5) interactions between the DBA molecules to stabilize the structure (Figure 1, bottom left). For 2–3 DBA molecules, the structures were unstable (i.e., the pores collapsed to $d_{001} < 6 \text{ \AA}$, thus making them inaccessible to gas adsorption, see Figure 3, left panel), requiring at least 4 DBA molecules to remain open, but in that case, the $d_{001} \approx 11\text{--}12.5 \text{ \AA}$ was also too large (and, as we shall see later, remarkably pressure independent, as expected for larger pores^{24–26}). To test if the problem was a finite-size effect, we doubled the xy dimensions of the simulation cell (quadrupling the GOF surface area), but the results were unchanged: the van der Waals GOFs resulted in either a collapsed pore or a very large and stable pore.

For model (iii) fDBA-GOF, we created GO by adding epoxy and hydroxyl groups randomly to graphene based on the Leref–Klinowski model^{46–48} and randomly placed 2–6 DBA molecules between the GO layers (see Figure 1, top right). We tested numerous randomly produced GO/fluid-DBA configurations, but the results were always the same: a complete collapse of the pores to interlayer distances $d_{001} < 7.8 \text{ \AA}$ that almost completely excluded any gas molecules from adsorbing inside the pore; see Figure 3, right panel.

Here, we propose a new fourth model (iv) CA-GOF, which retains the main characteristics of Burress⁹ but that is compatible with experimental observations of base layer spacing $d_{001} \approx 9.3 \text{ \AA}$ and, as we shall see below, shows adsorption isotherms and swelling of the interlayer spacing consistent with the experimental results of Schaeperkoetter et al.¹⁸ for both methane and xenon. The generalization is intuitive: instead of linking the DBAs perpendicularly to the graphene planes, we first covalently bond them (eq 2) to a random pair of C atoms in one layer of graphene (i.e., forming C–O bonds, it should be noted that the algorithm does not allow C–O bonds for different DBA molecules within the same graphene unit cell). Second, a random search is performed for a C–C bond in the second layer of graphene within the geometrical constraints to produce the desired layer spacings (i.e., the binding sites are displaced between 4.5 and 7.5 \AA in the graphene plane); see Figure 1, bottom right. In a typical simulation, we place three DBA molecules per simulation cell so that the boron content is comparable to that observed.^{9,11,18}

Initial energy minimization in NAMD2 is then performed to eliminate geometrically unstable configurations, in addition to eliminating those for which the starting pore spacing d_{001} ($N = 0$) differed by more than $\pm 0.5 \text{ \AA}$ from the experimental results (9.3 \AA). The idea is that the configurations that match the pore spacing of Schaeperkoetter et al.’s experiments¹⁸ are representative of the GOFs from the said experiments.

3.2. Determination of Interlayer Spacing d_{001} and Variation with Methane and Xenon Adsorption. We created VMD/TCL scripts to calculate the average pore spacing by finding the density of graphene carbon atoms at specific z -values of separation between pores $P(z)$. In the script, the first 1,000,000 MD steps of “thermalization” are discarded, and statistics was collected for the last 2,000,000 steps (2000 frames separated by 1 ps), as described in Section 2. Figure 4 shows variations of $P(z)$ distribution for some values of methane pressure P_{met} for one particular configuration of model (iv) “covalent angled GOF.” We observe that the density distribution $P(z)$ varies with the number of gas molecules (pressure) and, in general, we observe that the average pore spacing $d_{001} = \langle z \rangle$ increases with pressure as observed via neutron diffraction by Schaeperkoetter et al.¹⁸

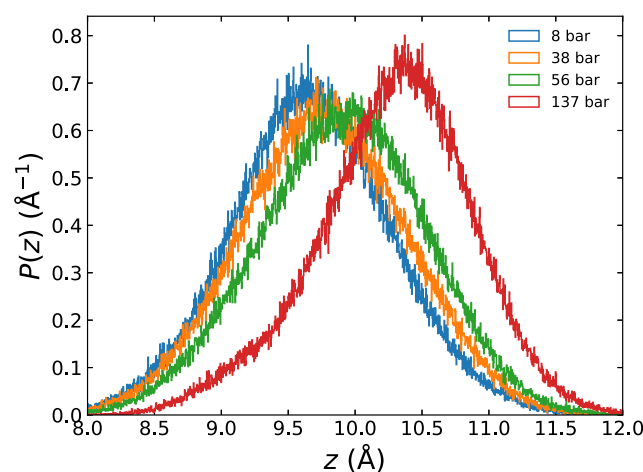


Figure 4. Height density plot of carbon atoms in the top layer of graphene in the simulated GOF relative to the bottom layer at various methane pressures for one typical “covalent angled GOF” configuration. We observe a gradual increase of the average pore spacing $d_{001} = \langle z \rangle$ with pressure similar to what is observed experimentally.¹⁸

We should note that since our structures were created at random, some resulted in pores that partially collapsed (e.g., because all DBA linkers were clustered in one small area)—these runs, as mentioned earlier, were discarded—it is thus important to remark that any conclusion must be drawn from analyzing averages of large ensembles of configurations. Figure 5 shows averages of d_{001} variations with methane pressure for

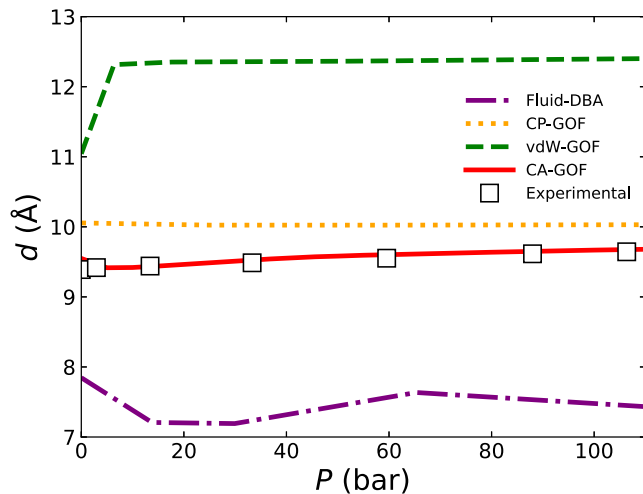


Figure 5. Pore spacing d_{001} calculated by averaging over numerous configurations for each of the discussed GOF-DBA models (Figure 1) and comparison with experimental results of Schaeperkoetter et al.¹⁸ Error bars of the experimental data are omitted because they are too small at this scale. The dispersion of the computational data is shown in Figure 6.

the four GOF-DBA models discussed in this paper. It is evident that the interlayer distance d_{001} for CP-GOF⁹ and vdW-GOF¹¹ are both too large (~ 10.3 , $11\text{--}12.5$ Å), and for fDBA-GOF¹¹ too small (7–8 Å, and excluding any gas from its interior) when compared to Schaeperkoetter's neutron diffraction results (9.3–9.75 Å).¹⁸ Only the proposed CA-GOF is consistent with experiments even before the small variation (in this scale) of d_{001} with methane pressure is discussed below.

In the case of the CA-GOF model proposed in this paper, the random arrangement of DBA molecules causes a range of possible distances between graphene sheets. For the distance between graphene sheets to be equal to the experimental distance, diborane bonds with two graphene layers must be shifted in the xy direction by ~ 6 Å. For our analysis, we picked structures with random shifts between 4.5 and 7.5 Å and discarded results in which geometries resulted in pores that collapsed. Figure 6 shows how the layer spacing $d_{001} = \langle z \rangle$ (see Figure 4) varies with the methane pressure for 32 random configurations color coded by how close they are to the low-pressure experimental spacing.¹⁸ It is evident that the results are quite dispersed. However, averaging over these configurations (thick lines in Figure 6) results in curves that are in reasonable agreement with neutron diffraction experiments,¹⁸ and unsurprisingly, the average calculated for the seven configurations closest to the experimental value has a better agreement than the more dispersed data set. A similar analysis was performed for the swelling of the interlayer spacing upon adsorption of xenon. The data set is more limited but shares the methane's characteristics.

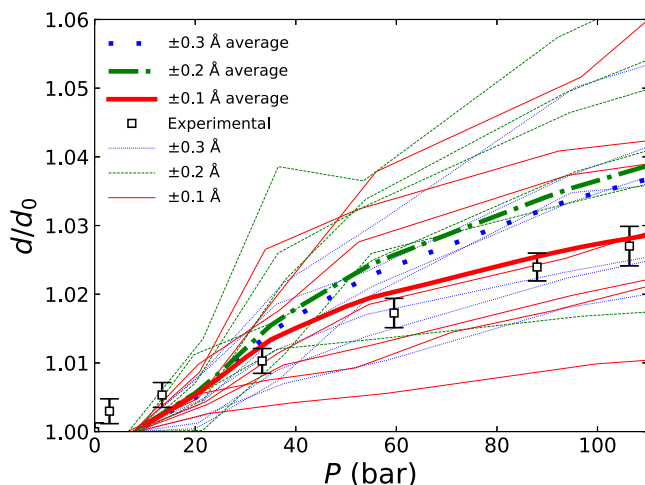


Figure 6. Pore spacing relative increase d/d_0 as a function of methane pressure P_{met} . Thin lines are individual configurations color coded by their low-pressure variation in d_{001} vs the experiment¹⁸ (note: $d_0 = 9.35$ Å). Thick lines represent averages within each class.

Figure 7 shows the variation of the layer spacing d_{001} as a function of pressure during adsorption of methane and xenon.

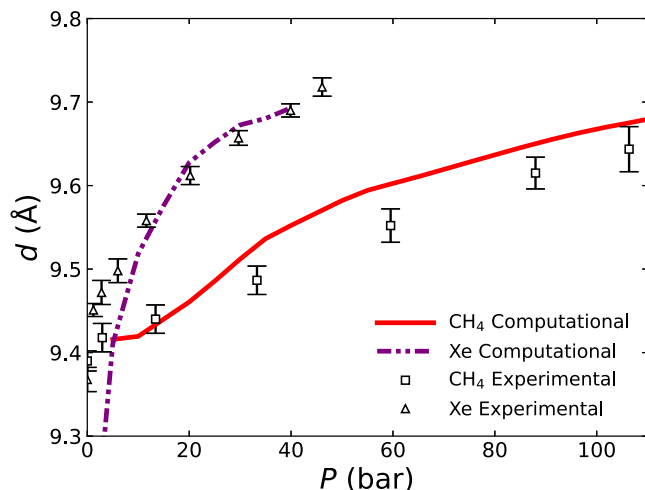


Figure 7. Pore spacing absolute increase of d_{001} as a function of methane and xenon pressure. Experimental data from Schaeperkoetter et al.¹⁸ The larger variation of d_{001} with the pressure for Xe was explained in ref 18 from the different gas interaction parameters.

The lines represent the *ensemble averages* of many GOF configurations as described above, and symbols are from Schaeperkoetter et al.'s *in situ* neutron diffraction experiments.¹⁸ Overall, the *ensemble average* variation of layer spacing with gas pressure for this model is in very reasonable agreement with experiments. The larger variation of d_{001} with pressure for Xe was explained in ref 18 from the different gas interaction parameters.

3.3. Adsorption Isotherms. We also created VMD/TCL scripts to compute the average number of gas molecules residing inside the pores to calculate the absolute adsorption isotherms for CA-GOF model structures (last 2000 frames, as in Section 3.2). The number of adsorbed molecules inside the GOF structure is averaged, while separately the gas pressure is calculated using NIST's Thermophysical Properties of Fluid Systems database³¹ from gas densities averaged far from the

GOF (and DBA), i.e., in the bottom 10 Å of the simulation box; see Figure 2³² Figure 8 shows the individual

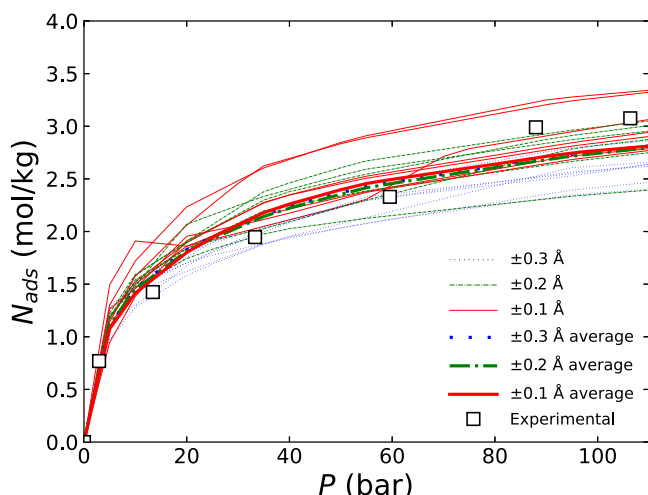


Figure 8. Absolute adsorption of methane in “covalent angled GOF” systems and their *ensemble averages* and experimental results.¹⁸ Figure 6 shows the color scheme.

configurations’ adsorption isotherms and their *ensemble averages* (see discussion in Section 3.2, Figure 6). Figure 9

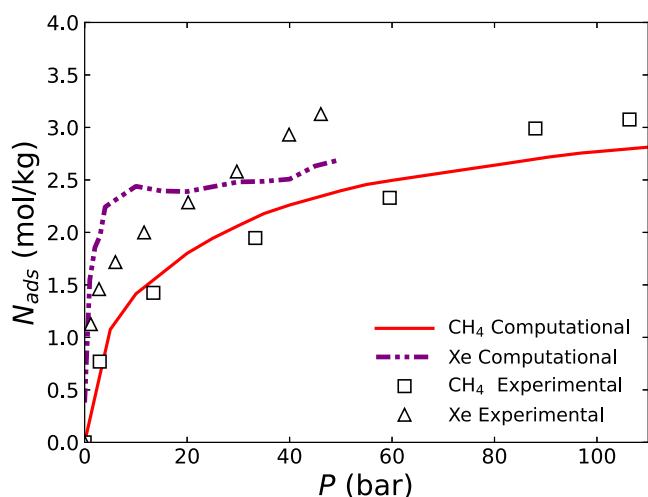


Figure 9. Absolute adsorption of methane and xenon in “covalent angled GOF” *ensemble averages* for the $\pm 0.1 \text{ \AA}$ tolerance level compared to experimental results.¹⁸

shows a comparison between the experimental and average simulated adsorption isotherms for methane and xenon. Xenon adsorbed noticeably more rapidly in the simulations than in Schaeperkoetter et al.’s¹⁸ experiments, but overall there is a reasonable agreement for both gases considering the large degree of variability in the simulated GOF structures.

4. DISCUSSION

Our observations of monotonic and gradual swelling of the d_{001} spacing for the CA-GOF model are consistent with Schaeperkoetter et al.’s observations.¹⁸ Perhaps the main criticism of any of the covalently bonded models (model i or iv, see Section 1) is by Mercier et al.:¹¹ they posit that because the pore size swells up to 15.4 Å when in water, the DBA

cannot be covalently linked as 12 Å would be the limit of the height.¹¹ However, an alternative explanation for the large swelling when flooded with a polar solvent may be boronate esterification, a well-studied reversible reaction^{49,50} where a boron bonded to two oxygen and a diol, in this case carbon, will have its oxygens detach from a surface such as graphene in the presence of water, leaving behind OH on the surface as the boron’s two newly detached oxygens each gain a hydrogen, all within a short time.⁵⁰ When the boronate’s oxygens bond back with the surface, the reaction produces water. If no water is present, the boronate remains bonded to the surface. Therefore, flooding the pores with water could, in theory, detach all DBA molecules and then swell the pores to distances too great for the DBAs to bond to both sides. Conversely, continuous heat-induced evaporation of water in a GOF will result in DBAs being only covalently bonded to the surface. In conclusion, it is possible for the covalently bonded models to be consistent with pore sizes swelling up to 15.4 Å.

The results of our covalent angled model support non-perpendicular covalent bonding sites for the DBA molecules. Because the *angle* and *dihedral* molecular degrees of freedom (eqs 3 and 4) are involved in the expansion—much “softer” than the *bond lengths* (eq 2), this enhances the flexibility of the framework and allows the expansion of the d_{001} spacing of the GOF. Although current diffraction techniques cannot verify the orientation of the DBA molecules, we suggest that the small changes to DBA–graphene bond site positions proposed in our covalent angled model are viable. The results suggest that the structure of the GOF is made up of DBA pillars randomly linked to the carbons of the graphene sheets. This implies that the GOF may not form a perfect three-dimensional network but may have some dispersion. Schaeperkoetter et al.¹⁸ observed GOF crystallite domains sizes of ~ 13.7 nm, a decrease of $\sim 20\%$ from GOs, which may support this picture. A more detailed analysis of how the crystallite domain size vary with the incorporation of DBA pillars and during adsorption may help clarify this point.

In conclusion, we have simulated the adsorption of three existing and one new models of GOF-DBA and find that only the model (iv) “covalent angled GOF” is compatible with the observed swelling of the d_{001} spacing during supercritical adsorption of methane and xenon. This should help the development of new structured porous materials for high-performance adsorption of gases and catalytic reactions.

■ ASSOCIATED CONTENT

SI Supporting Information

The Supporting Information is available free of charge at <https://pubs.acs.org/doi/10.1021/acsomega.2c00151>.

Detailed CHARMM22 force field used in the simulations of this paper and a description of the *ab initio* density functional theory method used to determine the parameters of the force field ([PDF](#))

■ AUTHOR INFORMATION

Corresponding Authors

Todd N. Lombardi — Department of Physics and Astronomy, University of Missouri, Columbia, Missouri 65211, United States; [ORCID: 0000-0002-4857-7867](https://orcid.org/0000-0002-4857-7867); Email: tnl285@mail.missouri.edu

Carlos Wexler — Department of Physics and Astronomy, University of Missouri, Columbia, Missouri 65211, United

States; orcid.org/0000-0002-7038-2628; Email: wexlerc@missouri.edu

Authors

Joseph C. Schaeperkoetter — Department of Physics and Astronomy, University of Missouri, Columbia, Missouri 65211, United States; University of Missouri Research Reactor, Columbia, Missouri 65211, United States; Kazuo Inamori School of Engineering, Alfred University, Alfred, New York 14802, United States; orcid.org/0000-0002-8794-5466

Alberto Albesa — Department of Physics and Astronomy, University of Missouri, Columbia, Missouri 65211, United States; Instituto de Investigaciones Fisicoquímicas Teóricas y Aplicadas, Departamento de Química, Universidad Nacional de La Plata, La Plata 1900, Argentina; orcid.org/0000-0002-7278-5789

Complete contact information is available at:
<https://pubs.acs.org/10.1021/acsomega.2c00151>

Notes

The authors declare no competing financial interest.

ACKNOWLEDGMENTS

The authors acknowledge useful discussions with Matthew Connolly, Haskell Taub, Helmut Kaiser, and Jacob Burress. This work was supported in part by the National Science Foundation Grant No. IIP-2044726.

REFERENCES

- (1) Golebiowska, M.; Roth, M.; Firlej, L.; Kuchta, B.; Wexler, C. The Reversibility of the Adsorption of Methane–Methyl Mercaptan Mixtures in Nanoporous Carbon. *Carbon* **2012**, *50*, 225–234.
- (2) Collins, S. P.; Perim, E.; Daff, T. D.; Skaf, M. S.; Galvão, D. S.; Woo, T. K. Idealized Carbon-Based Materials Exhibiting Record Deliverable Capacities for Vehicular Methane Storage. *J. Phys. Chem. C* **2019**, *123*, 1050–1058.
- (3) Szczęśniak, B.; Choma, J.; Jaroniec, M. Gas Adsorption Properties of Graphene-Based Materials. *Adv. Colloid Interface Sci.* **2017**, *243*, 46–59.
- (4) Dally, A.; Beckner, M. Methane Storage on Metal–Organic Frameworks. In *Nanoporous Materials for Gas Storage*; Springer: Singapore, 2019, Vol. 520; pp 227–253.
- (5) Pazoki, H.; Anbia, M. Synthesis of a Microporous Copper Carboxylate Metal Organic Framework as a New High Capacity Methane Adsorbent. *Polyhedron* **2019**, *171*, 108–111.
- (6) Bhatia, S. K.; Myers, A. L. Optimum Conditions for Adsorptive Storage. *Langmuir* **2006**, *22*, 1688–1700.
- (7) Kuchta, B.; Firlej, L.; Roszak, Sz. P.; Pfeifer; Wexler, C. Influence of Structural Heterogeneity of Nanoporous Sorbent Walls on Hydrogen Storage. *Appl. Surf. Sci.* **2010**, *256*, 5270–5274.
- (8) Herrera-Alonso, M.; Abdala, A. A.; McAllister, M. J.; Aksay, I. A.; Prud'homme, R. K. Intercalation and Stitching of Graphite Oxide with Diaminoalkanes. *Langmuir* **2007**, *23*, 10644–10649.
- (9) Burress, J. W.; Gadielli, S.; Ford, J.; Simmons, J. M.; Zhou, W.; Yildirim, T. Graphene Oxide Framework Materials: Theoretical Predictions and Experimental Results. *Angew. Chem., Int. Ed.* **2010**, *49*, 8902–8904.
- (10) Srinivas, G.; Burress, J. W.; Ford, J.; Yildirim, T. Porous Graphene Oxide Frameworks: Synthesis and Gas Sorption Properties. *J. Mater. Chem.* **2011**, *21*, 11323–11329.
- (11) Mercier, G.; Klechikov, A.; Hedenström, M.; Johnels, D.; Baburin, I. A.; Seifert, G.; Mysyk, R.; Talyzin, A. V. Porous Graphene Oxide/Diboronic Acid Materials: Structure and Hydrogen Sorption. *J. Phys. Chem. C* **2015**, *119*, 27179–27191.
- (12) Zhu, Y.; Murali, S.; Cai, W.; Li, X.; Suk, J. W.; Potts, J. R.; Ruoff, R. S. Graphene and Graphene Oxide: Synthesis, Properties, and Applications. *Adv. Mater.* **2010**, *22*, 3906–3924.
- (13) Kim, H.; Abdala, A. A.; Macosko, C. W. Graphene/Polymer Nanocomposites. *Macromolecules* **2010**, *43*, 6515–6530.
- (14) Putz, K. W.; Compton, O. C.; Palmeri, M. J.; Nguyen, S. T.; Brinson, L. C. High-Nanofiller-Content Graphene Oxide–Polymer Nanocomposites via Vacuum-Assisted Self-Assembly. *Adv. Funct. Mater.* **2010**, *20*, 3322–3329.
- (15) Dreyer, D. R.; Jia, H.-P.; Bielawski, C. W. Graphene Oxide: A Convenient Carbocatalyst for Facilitating Oxidation and Hydration Reactions. *Angew. Chem., Int. Ed.* **2010**, *49*, 6686.
- (16) Matsuo, Y.; Sakai, Y.; Fukutsuka, T.; Sugie, Y. Preparation of Pillared Carbons by Pyrolysis of Silylated Graphite Oxide. *Chem. Lett.* **2007**, *36*, 1050–1051.
- (17) Matsuo, Y.; Sakai, Y.; Fukutsuka, T.; Sugie, Y. Preparation and Characterization of Pillared Carbons Obtained by Pyrolysis of Silylated Graphite Oxides. *Carbon* **2009**, *47*, 804–811.
- (18) Schaeperkoetter, J. C.; Connolly, M. J.; Buck, Z. N.; Taub, H.; Kaiser, H.; Wexler, C. Adsorption-Induced Expansion of Graphene Oxide Frameworks: Observation by in Situ Neutron Diffraction. *ACS Omega* **2019**, *4*, 18668–18676.
- (19) Thomas, M.; Stansfield, R.; Berneron, M.; Filhol, A.; Greenwood, G.; Jacob, J.; Feltin, D.; Mason, S. *Position Sensitive Detection of Thermal Neutrons*, Edited by Convert, P.; Convert, P.; Forsyth, J. B., Eds.; 1983.
- (20) Hyun, S.; Lee, J. H.; Jung, G. Y.; Kim, Y. K.; Kim, T. K.; Jeoung, S.; Kwak, S. K.; Moon, D.; Moon, H. R. Exploration of Gate-Opening and Breathing Phenomena in a Tailored Flexible Metal–Organic Framework. *Inorg. Chem.* **2016**, *55*, 1920–1925.
- (21) Coudert, F.-X.; Mellot-Draznieks, C.; Fuchs, A. H.; Boutin, A. Prediction of Breathing and Gate-Opening Transitions Upon Binary Mixture Adsorption in Metal–Organic Frameworks. *J. Am. Chem. Soc.* **2009**, *131*, 11329–11331.
- (22) Russell, B.; Villaroel, J.; Sapag, K.; Migone, A. D. O₂ Adsorption on ZIF-8: Temperature Dependence of the Gate-Opening Transition. *J. Phys. Chem. C* **2014**, *118*, 28603–28608.
- (23) Nomura, K.; Nishihara, H.; Yamamoto, M.; Gabe, A.; Ito, M.; Uchimura, M.; Nishina, Y.; Tanaka, H.; Miyahara, M. T.; Kyotani, T. Force-Driven Reversible Liquid–Gas Phase Transition Mediated by Elastic Nanosponges. *Nat. Commun.* **2019**, *10*, No. 2559.
- (24) Neimark, A. V.; Coudert, F.-X.; Boutin, A.; Fuchs, A. H. Stress-Based Model for the Breathing of Metal–Organic Frameworks. *J. Phys. Chem. Lett.* **2010**, *1*, 445–449.
- (25) Gor, G. Yu.; Neimark, A. V. Adsorption-Induced Deformation of Mesoporous Solids. *Langmuir* **2010**, *26*, 13021–13027.
- (26) Ancilotto, F.; Cole, M. W.; Grosman, A.; Hernández, E. S.; Toigo, F. Expansion or Contraction of Slit Pores Due to Gas Uptake. *J. Low Temp. Phys.* **2011**, *163*, 284–301.
- (27) Quinn, D. F. Supercritical Adsorption of ‘Permanent’ Gases under Corresponding States on Various Carbons. *Carbon* **2002**, *40*, 2767–2773.
- (28) Kim, H.-Y.; Lueking, A. D.; Gatica, S. M.; Karl Johnson, J.; Cole, M. W. A Corresponding States Principle for Physisorption and Deviations for Quantum Fluids. *Mol. Phys.* **2008**, *106*, 1579–1585.
- (29) Phillips, J. C.; Hardy, D. J.; Maia, J. D. C.; Stone, J. E.; Ribeiro, J. V.; Bernardi, R. C.; Buch, R.; Fiorin, G.; Hénin, J.; Jiang, W.; McGreevy, R.; Melo, M. C. R.; Radak, B. K.; Skeel, R. D.; Singhary, A.; Wang, Y.; Roux, B.; Aksimentiev, A.; Luthey-Schulten, Z.; Kalé, L. V.; Schulten, K.; Chipot, C.; Tajkhorshid, E. Scalable Molecular Dynamics on CPU and GPU Architectures with NAMD. *J. Chem. Phys.* **2020**, *153*, No. 044130.
- (30) Humphrey, W.; Dalke, A.; Schulten, K. VMD: Visual Molecular Dynamics. *J. Mol. Graph.* **1996**, *14*, 33–38.
- (31) Lemmon, E. W.; McLinden, M. O.; Friend, D. G. Thermophysical Properties of Fluid Systems. In *NIST Chemistry WebBook, NIST Standard Reference Database Number 69*; National Institute of Standards and Technology: Gaithersburg MD, 20899.

- (32) Valleroy, Z.; dos Santos, G.; Lombardi, T.; Wexler, C. Adsorption of Natural Gas Mixtures of Methane, Ethane, and Propane in Nanoporous Carbon: Fully Atomistic Numerical Studies. *Langmuir* **2020**, *36*, 3690–3702.
- (33) Brooks, B. R.; Bruccoleri, R. E.; Olafson, B. D.; States, D. J.; Swaminathan, S.; Karplus, M. CHARMM: A Program for Macromolecular Energy, Minimization, and Dynamics Calculations. *J. Comput. Chem.* **1983**, *4*, 187–217.
- (34) Andersen, H. C. Rattle: A “Velocity” Version of the Shake Algorithm for Molecular Dynamics Calculations. *J. Comput. Phys.* **1983**, *52*, 24–34.
- (35) Amaro, R.; Dhaliwal, B.; Luthey-Schulten, Z. *Computational Biophysics Workshop*; University of Illinois: Urbana-Champaign, 2007.
- (36) Firlej, L.; Kuchta, B.; Roth, M. W.; Wexler, C. Molecular Simulations of Intermediate and Long Alkanes Adsorbed on Graphite: Tuning of Non-Bond Interactions. *J. Mol. Model.* **2011**, *17*, 811–816.
- (37) MacKerell, A. D.; Bashford, D.; Bellott, M.; Dunbrack, R. L.; Evanseck, J. D.; Field, M. J.; Fischer, S.; Gao, J.; Guo, H.; Ha, S.; Joseph-McCarthy, D.; Kuchnir, L.; Kuczera, K.; Lau, F. T. K.; Mattos, C.; Michnick, S.; Ngo, T.; Nguyen, D. T.; Prodhom, B.; Reiher, W. E.; Roux, B.; Schlenkrich, M.; Smith, J. C.; Stote, R.; Straub, J.; Watanabe, M.; Wiórkiewicz-Kuczera, J.; Yin, D.; Karplus, M. All-Atom Empirical Potential for Molecular Modeling and Dynamics Studies of Proteins. *J. Phys. Chem. B* **1998**, *102*, 3586–3616.
- (38) Ewald, P. P. Die Berechnung Optischer Und Elektrostatischer Gitterpotentiale. *Ann. Phys.* **1921**, *369*, 253–287.
- (39) Becke, A. D. Density-functional Thermochemistry. III. The Role of Exact Exchange. *J. Chem. Phys.* **1993**, *98*, 5648–5652.
- (40) Lee, C.; Yang, W.; Parr, R. G. Development of the Colle-Salvetti Correlation-Energy Formula into a Functional of the Electron Density. *Phys. Rev. B* **1988**, *37*, 785–789.
- (41) Vosko, S. H.; Wilk, L.; Nusair, M. Accurate Spin-Dependent Electron Liquid Correlation Energies for Local Spin Density Calculations: A Critical Analysis. *Can. J. Phys.* **1980**, *58*, 1200–1211.
- (42) Stephens, P. J.; Devlin, F. J.; Chabalowski, C. F.; Frisch, M. J. Ab Initio Calculation of Vibrational Absorption and Circular Dichroism Spectra Using Density Functional Force Fields. *J. Phys. Chem. A* **1994**, *98*, 11623–11627.
- (43) Frisch, M. J.; Trucks, G. W.; Schlegel, H. B.; Scuseria, G. E.; Robb, M. A.; Cheeseman, J. R.; Scalmani, G.; Barone, V.; Mennucci, B.; Petersson, G. A.; Nakatsuji, H.; Caricato, M.; Li, X.; Hratchian, H. P.; Izmaylov, A. F.; Bloino, J.; Zheng, G.; Sonnenberg, J. L.; Hada, M.; Ehara, M.; Toyota, K.; Fukuda, R.; Hasegawa, J.; Ishida, M.; Nakajima, T.; Honda, Y.; Kitao, O.; Nakai, H.; Vreven, T.; Montgomery, J. A., Jr.; Peralta, J. E.; Ogliaro, F.; Bearpark, M.; Heyd, J. J.; Brothers, E.; Kudin, K. N.; Staroverov, V. N.; Kobayashi, R.; Normand, J.; RagHAVACHARI, K.; Rendell, A.; Burant, J. C.; Iyengar, S. S.; Tomasi, J.; Cossi, M.; Rega, N.; Millam, J. M.; Klene, M.; Knox, J. E.; Cross, J. B.; Bakken, V.; Adamo, C.; Jaramillo, J.; Gomperts, R.; Stratmann, R. E.; Yazyev, O.; Austin, A. J.; Cammi, R.; Pomelli, C.; Ochterski, J. W.; Martin, R. L.; Morokuma, K.; Zakrzewski, V. G.; Voth, G. A.; Salvador, P.; Dannenberg, J. J.; Dapprich, S.; Daniels, A. D.; Farkas, Ö.; Foresman, J. B.; Ortiz, J. V.; Cioslowski, J.; Fox, D. J. *Gaussian~09*, Revision E.01.
- (44) Vanommeslaeghe, K.; MacKerell, A. D. Automation of the CHARMM General Force Field (CGenFF) I: Bond Perception and Atom Typing. *J. Chem. Inf. Model.* **2012**, *52*, 3144–3154.
- (45) Vanommeslaeghe, K.; Raman, E. P.; MacKerell, A. D. Automation of the CHARMM General Force Field (CGenFF) II: Assignment of Bonded Parameters and Partial Atomic Charges. *J. Chem. Inf. Model.* **2012**, *52*, 3155–3168.
- (46) Lerf, A.; He, H.; Riedl, T.; Forster, M.; Klinowski, J. ¹³C and ¹H MAS NMR Studies of Graphite Oxide and Its Chemically Modified Derivatives. *Solid State Ionics* **1997**, *101–103*, 857–862.
- (47) He, H.; Riedl, T.; Lerf, A.; Klinowski, J. Solid-State NMR Studies of the Structure of Graphite Oxide. *J. Phys. Chem. B* **1996**, *100*, 19954–19958.
- (48) He, H.; Klinowski, J.; Forster, M.; Lerf, A. A New Structural Model for Graphite Oxide. *Chem. Phys. Lett.* **1998**, *287*, 53–56.
- (49) Hall, D. G. *Boronic Acids: Preparation, Applications in Organic Synthesis and Medicine*; John Wiley & Sons, 2006.
- (50) Sana, M.; Leroy, G.; Wilante, C. Enthalpies of Formation and Bond Energies in Lithium, Beryllium, and Boron Derivatives. A Theoretical Attempt for Data Rationalization. *Organometallics* **1991**, *10*, 264–270.

□ Recommended by ACS

Flexible Polypyrrole-Coated Polyamide Based Mats for Broadband Microwave Absorption and Electromagnetic Interference Shielding with Low Reflection

Yugen Wang, Shengyao Zhao, *et al.*

MARCH 23, 2023

ACS APPLIED POLYMER MATERIALS

READ ▶

Bonding of Neuropeptide Y on Graphene Oxide for Drug Delivery Applications to the Central Nervous System

Giada Cellot, Laura Ballerini, *et al.*

DECEMBER 02, 2022

ACS APPLIED NANO MATERIALS

READ ▶

Enhanced Water Evaporation from \AA -Scale Graphene Nanopores

Wan-Chi Lee, Kumar Varoon Agrawal, *et al.*

AUGUST 24, 2022

ACS NANO

READ ▶

Boosting Osmotic Energy Conversion of Graphene Oxide Membranes via Self-Exfoliation Behavior in Nano-Confinement Spaces

Yijun Qian, Weiwei Lei, *et al.*

JULY 22, 2022

JOURNAL OF THE AMERICAN CHEMICAL SOCIETY

READ ▶

Get More Suggestions >